Ultrafast Light Switching of Ferromagnetism in EuSe

A. B. Henriques,[1] X. Gratens,[1] P. A. Usachev,[1,*] V. A. Chitta,[1] and G. Springholz[2]
[1]*Instituto de Física, Universidade de São Paulo (USP), 05508-090 São Paulo, Brazil*
[2]*Institut für Halbleiter und Festkörperphysik, Johannes Kepler Universität (JKU) Linz, 4040 Linz, Austria*

(Received 21 February 2018; published 23 May 2018)

We demonstrate that light resonant with the band gap forces the antiferromagnetic semiconductor EuSe to enter ferromagnetic alignment in the picosecond timescale. A photon generates an electron-hole pair, whose electron forms a supergiant spin polaron of magnetic moment of nearly 6000 Bohr magnetons. By increasing the light intensity, the whole of the illuminated region can be fully magnetized. The key to the novel large photoinduced magnetization mechanism is the huge enhancement of the magnetic susceptibility when both antiferromagnetic and ferromagnetic interactions are present in the material and are of nearly equal magnitude, as is the case in EuSe.

DOI: 10.1103/PhysRevLett.120.217203

Control of the magnetic state of matter lies at the root of information storage technology and novel spintronic functionalities for continuing computer performance evolution [1]. Finding new and ever faster mechanisms of such control is a topic of vast current interest for the development of devices and for advancing knowledge in the field of light-matter interaction [2–5]. Here we report on the discovery of an ultrafast mechanism of light switching of antiferromagnetic EuSe into the ferromagnetic phase, which is efficient in the proximity of its Néel temperature.

The EuSe samples were grown by molecular beam epitaxy onto (111) BaF_2 substrates. Because of the almost perfect lattice constant matching ($a = 6.191$ Å and $a = 6.196$ Å for EuSe and BaF_2, respectively), nearly unstrained bulklike EuSe reference layers with micrometer thickness were obtained directly by growth on BaF_2. The time-resolved photoinduced Faraday rotation was measured by a two-color pump-probe technique using 2 ps light pulses, produced by a cavity-dumped titanium-sapphire mode-locked laser coupled to a second harmonic generator, as illustrated in Fig. 1. The Faraday rotation angle of the probe light pulse, $\Delta\theta_F$, induced by the pump pulse, was measured using lock-in techniques with a resolution better than 10^{-7} rad. The image of the excitation spot on the sample had a diameter of 150 μm, about twice the diameter of the probe spot. For continuous wave (cw) measurements, the same setup was used, except that the pump source was a doubled Nd:Yag laser or a Xe lamp coupled to a monochromator, and the probe source was a semiconductor laser of energy below the EuSe band gap of 2.0 eV. All measurements were performed using an optical cryostat containing a superconducting coil for magnetic fields up to 8 T, applied in the Faraday geometry. Figure 2 shows the photoinduced Faraday rotation (PFR) as a function of the applied magnetic field, for cw excitation with an intensity of $p = 400$ mW/cm^{-2}, at $T = 12$ K. The PFR signal has all the characteristics expected for photoinduced magnetic polarons: no signal at zero magnetic field, because polarons are randomly oriented and produce zero magnetization, and a very rapid increase when a magnetic field is applied, due to the complete alignment of the polaron ensemble along the field due to the Zeeman torque acting on particles with a large magnetic moment. Figure 2 shows that, when the applied magnetic field is increased beyond 1 T, the PFR effect gradually decreases towards zero; this is because large magnetic fields progressively force the EuSe lattice spins into ferromagnetic order, and ultimately the formation of spin polarons is quenched. Figure 3 shows that the PFR signal vanishes if the excitation photon energy is less than the band gap and increases abruptly at the band gap energy, demonstrating that the PFR effect is associated with photogenerated conduction band electrons.

Because the photoexcited electrons are bound to very heavy photoexcited holes [6], the spin polarons are immobile and are confined to a layer below the surface of the

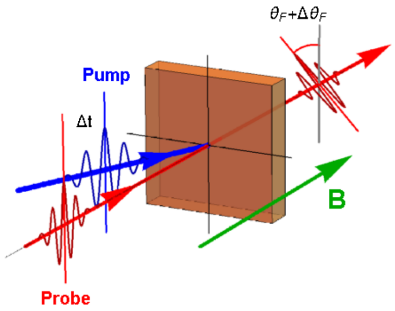

FIG. 1. Scheme of the setup for measuring the time-resolved photoinduced Faraday rotation angle. The linearly polarized probe pulse arrives at the sample when a time Δt has elapsed after the arrival of the pump pulse. We measured $\Delta\theta_F$, the increment in the Faraday rotation of the probe, induced by the pump illumination.

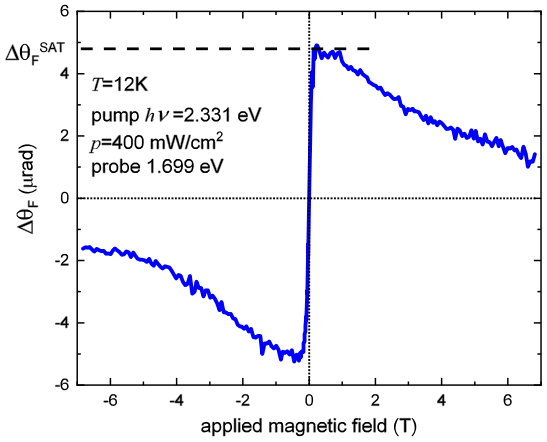

FIG. 2. Photoinduced Faraday rotation associated with spin polarons in EuSe. The maximum PFR is indicated by $\Delta\theta_F^{\mathrm{SAT}}$.

crystal whose thickness equals the penetration depth of the excitation light, $1/\alpha$, where $\alpha \cong 15\ \mu\mathrm{m}^{-1}$ is the EuSe absorption coefficient for the excitation photon energy [6]. From elementary kinetics, the steady-state density of photoinduced polarons is given by [7]

$$n_{\mathrm{pol}} = \chi \frac{p\alpha\tau_{\mathrm{pol}}}{h\nu} \leq \frac{p\alpha\tau_{\mathrm{pol}}}{h\nu}, \tag{1}$$

where $\chi \leq 1$ is the quantum efficiency for spin polaron photogeneration and τ_{pol} is the spin polaron lifetime. The spin polaron lifetime was deduced from the dependence of the PFR amplitude on the modulation frequency of the excitation light, shown in Fig. 4, following the procedure described in Ref. [8], giving $\tau_{\mathrm{pol}} = 1.6\ \mu$sec. The mean distance between polarons, d, in units of the EuSe lattice constant, is therefore

$$\frac{d}{a} \geq \frac{2}{a}\left(\frac{3}{4\pi}\frac{h\nu}{p\alpha\tau_{\mathrm{pol}}}\right)^{1/3}. \tag{2}$$

Substituting all parameters into (2), we obtain $d_{\mathrm{pol}} \geq 36a$. Thus, d is at least one order of magnitude greater than the typical radius of a spin polaron in europium chalcogenide [9], $R_{\mathrm{pol}} \sim 3a$. Being so far apart, the polarons are noninteracting. Moreover, above the Néel temperature, the orientation of a spin polaron floats freely; therefore, an ensemble of spin polarons forms a superparamagnetic gas, whose magnetization dependence on the magnetic field and temperature obeys a Langevin function [10]. Because PFR is proportional to the magnetization [11], the photoinduced Faraday rotation angle will be given by

$$\Delta\theta_F = \Delta\theta_F^{\mathrm{SAT}} L\left(\frac{\mu_{\mathrm{pol}} B}{k_B T}\right), \tag{3}$$

where $L(x) = \coth(x) - 1/x$ is the Langevin function.

The magnitude of the magnetic moment of the spin polaron at a given temperature can be determined accurately by fitting the experimental curve with (3), because it is the sole adjustable parameter determining the sharpness of the step. However, we must first convert the applied magnetic field into an internal one, which is smaller than the former due to the demagnetizing field [12]. For the Faraday geometry used here, where the magnetic field is normal to a very thin epitaxial layer, the ratio of the internal magnetic field to the applied one is equal to the ratio of the magnetic susceptibility measured when the applied field is perpendicular to the layer ($\chi_\perp$) to the susceptibility measured when the applied field is parallel to it ($\chi_\parallel$). The susceptibilities $\chi_\perp$ and $\chi_\parallel$ were measured using a SQUID magnetometer, which had a magnetic moment resolution better than 10^{-11} A m^2. Figure 5 shows the measured PFR as a function of the internal magnetic field. The inset shows the measured ratio between susceptibilities $\chi_\perp$ and $\chi_\parallel$, used to convert the applied magnetic field into an internal one, above the Néel temperature, $T_N = 4.75$ K (see the inset in Fig. 5, where T_N is indicated). The solid line in Fig. 5

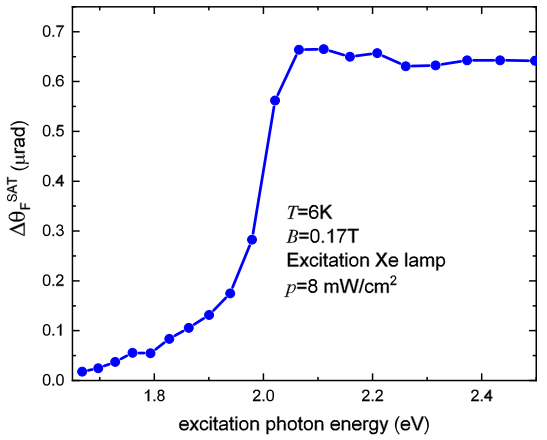

FIG. 3. PFR excitation spectrum.

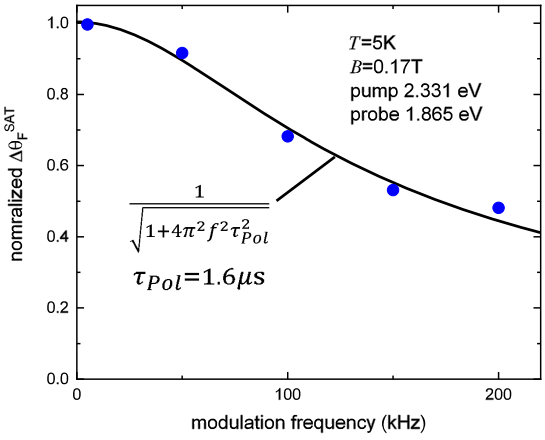

FIG. 4. PFR as a function of the pump modulation frequency.

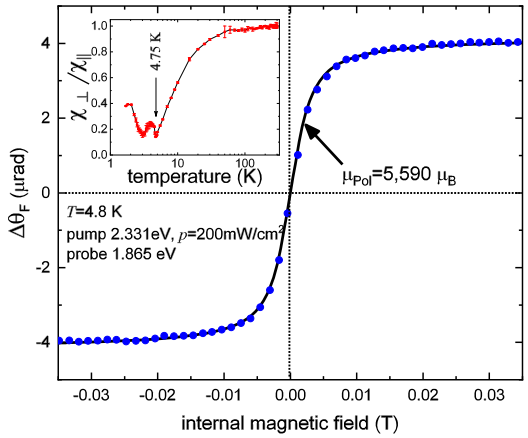

FIG. 5. PFR associated with spin polarons as a function of the internal magnetic field. The ratio $\chi_\perp/\chi_{||}$, used to compute the internal magnetic field, is shown in the inset, as a function of the temperature. The arrow in the inset indicates the Néel temperature for the sample studied, $T_N = 4.75$ K.

shows the fit of the theory, using (3), which yields the magnetic moment of the spin polaron, $\mu_{\rm pol} = 5590$ Bohr magnetons (μ_B). This magnetic moment is 10 times greater than the giant photoinduced spin polarons known so far [7,8], which allows us to categorize the spin polarons discovered as supergiant.

The magnetic moment of the spin polaron as a function of the temperature is shown in Fig. 6. Increasing the temperature quenches spin polaron formation, due to the decreasing magnetic susceptibility of the lattice spins. At temperatures much higher than the Néel temperature, when $\mu_{\rm Eu}B/k_BT \ll 1$, the magnetization of lattice spins can be well described by the paramagnetic approximation

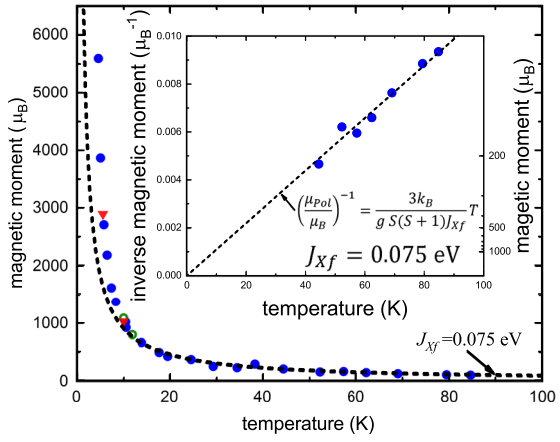

FIG. 6. Magnetic moment of a photoinduced polaron as a function of the temperature. Full circles, empty circles, and inverted triangles correspond to probe energies of 1.865, 1.699, and 1.632 eV, respectively. The dashed line shows the paramagnetic approximation, with $J_{\rm Xf} = 0.075$ eV obtained from the linear fit shown in the inset.

$$M = N\mu_{\rm Eu}\frac{S+1}{3S}\frac{\mu_{\rm Eu}B}{k_BT}, \tag{4}$$

where $N = 4/a^3$ is the density of Eu sites in the crystal and $\mu_{\rm Eu} = g\mu_B S$ is the magnetic moment of an Eu atom, where $g = 2$ and $S = 7/2$. The exchange interaction between the photoexcited electron, whose wave function is $\psi(r)$, and the lattice Eu spins is described by an effective magnetic field, $B_{\rm Xf}$, acting on the lattice spins [13]

$$B_{\rm Xf} = \frac{J_{\rm Xf}S}{N\mu_{\rm Eu}}|\psi(r)|^2, \tag{5}$$

where $J_{\rm Xf}$ is the exchange interaction integral between the electron forming the spin polaron and the lattice spins [9]. Substituting (5) in (4), and integrating in the whole volume, the high-temperature magnetic moment of a spin polaron in the paramagnetic crystal approximation is obtained:

$$\mu_{\rm pol}(T) = g\mu_B S(S+1)\frac{J_{\rm Xf}}{3k_BT}. \tag{6}$$

A fit of the high-temperature tail, $T > 40$ K, of $\mu_{\rm pol}$ versus T with (6), whereby $J_{\rm Xf}$ is the only adjustable parameter, is shown in the inset in Fig. 6 and gives $J_{\rm Xf} = 75$ meV. This $J_{\rm Xf}$ value is about the same as measured for EuTe by photoluminescence, meaning that the mean exchange field generated by the photoexcited electron in EuSe is about the same as for EuTe, i.e., about 1 T [9].

Figure 6 shows that, when the temperature is decreased below 20 K and approaches the Néel temperature, $\mu_{\rm pol}$ increases much faster than the paramagnetic approximation and can reach *almost an order of magnitude greater* than $\mu_{\rm pol}$ that would be observed if the exchange interaction was switched off (the paramagnetic approximation). This is in sharp contrast to EuTe, where $\mu_{\rm pol}$ *is always smaller* than the paramagnetic limit [8]. The reason for the very large increase in EuSe is the near equal absolute values of the first and second neighbor exchange interaction constants, J_1 and J_2. Whereas $J_1 > 0$ favors ferromagnetism, $J_2 < 0$ favors antiferromagnetism, which predominates only because $|J_2|$ is marginally larger than $|J_1|$. This also implies that around the Néel temperature only a very small internal magnetic field of about 0.1 T is sufficient to promote a phase transition into the ferromagnetic state, as demonstrated experimentally in Ref. [14]. Bearing in mind that within a spin polaron the effective magnetic field acting on the spins is about 1 T, this implies that within the polaron the crystal lattice attains ferromagnetic alignment, which explains why the magnetic moment of the polaron is so large in EuSe. Such reasoning is supported quantitatively by the Weiss mean field approximation (MFA) with first and second neighbor interaction at $T = 0$ K, according to which in the AFM-II phase: (1) the magnetic field required to induce ferromagnetic alignment is given by [9,13,15]

TABLE I. EuSe and EuTe parameters, μ_{pol} measured at $T = 5$ K and estimated using the MFA for $T = 0$ K.

				$\mu_{\mathrm{pol}}(\mu_B)$	
	J_1 (K)	J_2 (K)	J_{Xf} (eV)	Experiment	MFA
EuTe	0.043	−0.15	0.083	610	750
Reference	[18]		[13]	[7,13]	
EuSe	0.29	−0.30	0.075	5590	7300
Reference	[19]		This work		

$$B_{\mathrm{SAT}} = \frac{24|J_1 + J_2|S}{g\mu_B}; \tag{7}$$

(2) in the range $B < B_{\mathrm{SAT}}$ the magnetization is given by $M = N\mu_{\mathrm{Eu}}B/B_{\mathrm{SAT}}$ [16]. Using (5) and (7) and integrating M in the volume, the magnetic moment of the spin polaron in the mean field approximation is obtained:

$$\mu_{\mathrm{pol}}^{\mathrm{MFA}}(T = 0\ \mathrm{K}) = \frac{J_{\mathrm{Xf}}}{24|J_1 + J_2|}\, g\mu_B. \tag{8}$$

Table I displays the result produced by formula (8) for EuTe and EuSe. The calculated values agree by an order of magnitude with the measured values and demonstrate that the very large μ_{pol} in EuSe is due to the near cancellation of the ferro- and antiferromagnetic lattice interactions. This cancellation is exactly what makes EuSe so special in contrast to its parent compound EuTe, where the AFM lattice interaction is overwhelming, which leads to a much smaller spin polaron magnetic moment, as shown in Table I. The very large magnetic susceptibility in EuSe has already been exploited to construct tunneling junctions, which produce almost 100% spin-polarized currents [17].

The MFA does not provide any information about the internal structure of the spin polaron. A more accurate description of the spin polaron for the AFM-II phase at $T = 0$ K, and a description of its internal structure, is provided by a self-consistent calculation [13]. In performing such a calculation for EuSe, the input parameters were a conduction band effective mass $m^* = 0.3m_0$ [20] and a dielectric constant $\varepsilon = 9.4$ [21], as well as the parameters given in Table I. The self-consistent calculation produces a spin polaron with a large ferromagnetic core of radius 2.8 lattice parameters, containing 370 ferromagnetically aligned Eu atoms, with a calculated spin polaron of magnetic moment of $\mu_{\mathrm{pol}} = 4920\mu_B$.

Figure 7 shows $\Delta\theta_F^{\mathrm{SAT}}$, and the corresponding polaron population, deduced using the Verdet constant as described in Ref. [11], as a function of the excitation pump power density. The solid line is a fit using (1) with χ as the only fitting parameter, which yields $\chi = 0.06$. In dramatic contrast to EuTe, which shows a saturation of the polaron population, in EuSe the population grows linearly with excitation even at concentrations far above the expected residual defect concentrations, indicating that the photo-induced polarons are intrinsic, and therefore it should be possible to fully magnetize the layer penetrated by light simply by using enough excitation power. The maximum pump intensity shown in Fig. 7 generated about 2×10^{17} cm^{-3} spin polarons, and, taking into account their ferromagnetic core radius of about $3a$, this corresponds to a magnetization of 5×10^{-3} of the saturation value. We could not exploit greater pump intensities without heating of the sample, because we used an optical chopper with a high (50%) duty cycle.

Figure 8 shows the PFR signal as a function of the delay, Δt, between the pump and probe pulses (Fig. 1). Before the arrival of the pump pulse (negative delay), no PFR signal is detected; however, after the arrival of the pump pulse, the PFR signal grows exponentially with a characteristic rise time of 62 ps, which classifies the photomagnetization process as ultrafast. After achieving the maximum, the PFR remained approximately constant within the maximum

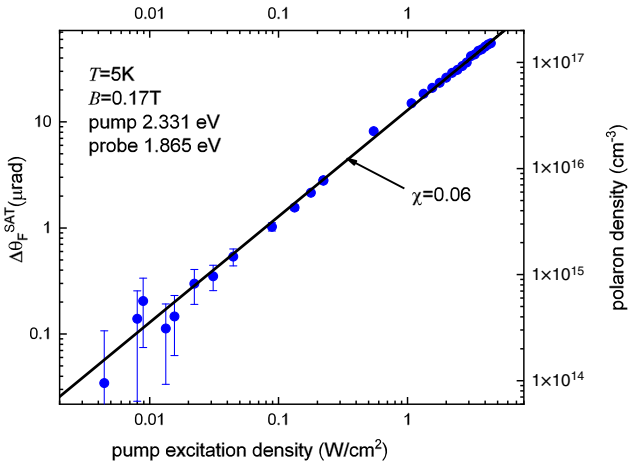

FIG. 7. PFR as a function of the pump excitation power.

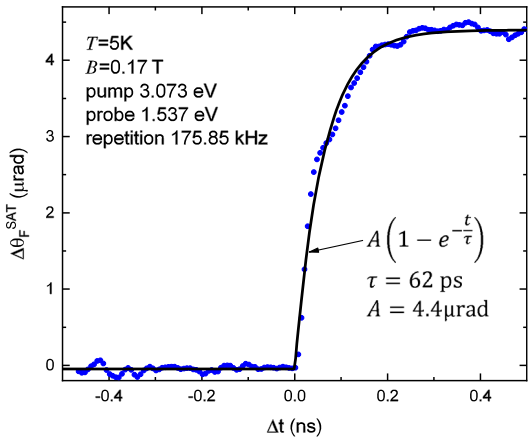

FIG. 8. PFR as a function of the delay, Δt, between the pump and probe pulses.

delay available of our experiment, of a few nanoseconds, which is explained by the long lifetime of the polarons, $\tau_{pol} = 1.6\ \mu$s, reported above. The characteristic rise time of 62 ps is a measure of the time required for the organization of the Eu lattice spins within the radius of the exciton, and it agrees by an order of magnitude with the rise time of 200 ps found for spin polaron creation in diluted magnetic semiconductors [22].

In conclusion, we have demonstrated that light can be used to convert a zero magnetization state of a EuSe crystal into a completely polarized ferromagnetic state in the ultrafast timescale, through the photogeneration of supergiant intrinsic spin polarons. This magnetization mechanism is made possible because the exchange interaction between lattice spins in EuSe contains both ferromagnetic and antiferromagnetic components, which nearly cancel each other out.

We thank Olimpio Ribeiro da Fonseca Neto for technical support. A. B. H. is grateful to Professor Günther Bauer for encouraging the cooperation between USP and JKU. This work was supported by the Brazilian agencies CNPq (Grant No. 304685/2010-0) and FAPESP (Grant No. 2016/24125-5), and the Austrian Science Funds Project No. P30960.

*Permanent address: Ioffe Institute, 194021 St. Petersburg, Russia.

[1] *Spintronics-based Computing*, edited by W. Zhao and G. Prenat (Springer International, Switzerland, 2015).
[2] Upping the anti, Nat. Phys. **14**, 199(E) (2018).
[3] J. Xie, H. Qin, Y. Hao, B.Cheng, W. Liu, L. Liu, S. Ren, G. Zhou, Z. Ji, and J. Hu, Sci. Rep. **7**, 45642 (2017).
[4] T. Satoh, R. Iida, T. Higuchi, Y. Fujii, A. Koreeda, H. Ueda, T. Shimura, K. Kuroda, V. I. Butrim, and B. A. Ivanov, Nat. Commun. **8**, 638 (2017).
[5] I. Radu *et al.*, Nature (London) **472**, 205 (2011).
[6] A. B. Henriques, A. Wierts, M. A. Manfrini, G. Springholz, P. H. O. Rappl, E. Abramof, and A. Y. Ueta, Phys. Rev. B **72**, 155337 (2005).
[7] A. B. Henriques, A. R. Naupa, P. A. Usachev, V. V. Pavlov, P. H. O. Rappl, and E. Abramof, Phys. Rev. B **95**, 045205 (2017).
[8] A. B. Henriques, G. D. Galgano, P. H. O. Rappl, and E. Abramof, Phys. Rev. B **93**, 201201 (2016).
[9] A. B. Henriques, G. D. Galgano, E. Abramof, B. Diaz, and P. H. O. Rappl, Appl. Phys. Lett. **99**, 091906 (2011).
[10] C. P. Bean and J. D. Livingston, J. Appl. Phys. **30**, S120 (1959).
[11] A. B. Henriques and P. A. Usachev, Phys. Rev. B **96**, 195210 (2017).
[12] S. Blundell, *Magnetism in Condensed Matter* (Oxford University, New York, 2001), Appendix D.
[13] A. B. Henriques, F. C. D. Moraes, G. D. Galgano, A. J. Meaney, P. C. M. Christianen, J. C. Maan, E. Abramof, and P. H. O. Rappl, Phys. Rev. B **90**, 165202 (2014).
[14] R. T. Lechner, G. Springholz, T. U. Schülli, J. Stangl, T. Schwarzl, and G. Bauer, Phys. Rev. Lett. **94**, 157201 (2005).
[15] W. Söllinger, W. Heiss, R. T. Lechner, K. Rumpf, P. Granitzer, H. Krenn, and G. Springholz, Phys. Rev. B **81**, 155213 (2010).
[16] L. K. Hanamoto, A. B. Henriques, N. F. Oliveira, P. Rappl, E. Abramof, and Y. Ueta, J. Phys. Condens. Matter **16**, 5597 (2004).
[17] J. S. Moodera, R. Meservey, and X. Hao, Phys. Rev. Lett. **70**, 853 (1993).
[18] P. Wachter, CRC Crit. Rev. Solid State Sci. **3**, 189 (1972).
[19] X. Gratens *et al.* (unpublished).
[20] S. J. Cho, Phys. Rev. B **1**, 4589 (1970).
[21] A. Mauger and C. Godart, Phys. Rep. **141**, 51 (1986).
[22] D. D. Awschalom, J. M. Halbout, S. von Molnár, T. Siegrist, and F. Holtzberg, Phys. Rev. Lett. **55**, 1128 (1985).